Quantum phase-space structures in classically mixed systems: a scattering approach

1997 J. Phys. A: Math. Gen. 30 3613

(http://iopscience.iop.org/0305-4470/30/10/033)

J. Phys. A: Math. Gen. **30** (1997) 3613–3634. Printed in the UK PII: S0305-4470(97)77989-7

Quantum phase-space structures in classically mixed systems: a scattering approach

Steffen D Frischat and Eyal Doron†

Max-Planck-Institut für Kernphysik, Postfach 103980, D-69029 Heidelberg, Germany

Received 19 September 1996

Abstract. The structure of quantum wavefunctions is discussed for a billiard system with mixed classical dynamics. Using a scattering formalism, we introduce a Husimi-like distribution for S-matrix eigenvectors at arbitrary wavenumbers, k (not necessarily eigenenergies of the system). This constitutes $N \propto k$ probability density plots on the Poincaré surface of section at any k. Many eigenvectors are structured by classical objects such as invariant tori, the intermediate layer between regular and chaotic motion, and unstable periodic orbits ('scars'). We find that eigenvector structure is stable over significant energy ranges, while the associated eigenphases increase linearly with k at a rate determined by the underlying classical objects. Additionally, we observe that in the presence of time-reversal symmetry, eigenvectors scarred by non-self-retracing periodic orbits form doublets which are closely spaced in eigenphase.

Our results provide a new perspective on the quantization of structured states: *quantization* is determined by the linearly increasing eigenphases, and occurs whenever an eigenphase is equal to $2\pi M$, while *structure* is encoded in the eigenvectors; it is present at all energies and varies only slowly. This allows one to predict many quantized eigenfunctions over an entire energy range by studying the eigenparameters of $\mathbf{S}$ at a *single* intermediate energy, and identifying the underlying classical objects.

1. Introduction

While most of the work in quantum chaos has centred around the spectral properties of classically chaotic systems, the structure of wavefunctions has also been of interest. This has mostly been in the form of the study of eigenfunctions of systems which are strongly chaotic, and one of the more intriguing effects which is observed is the presence of states which seem to be highly correlated with specific unstable periodic orbits. This phenomenon, dubbed 'scars', was originally described in [1, 2], and has since been observed in a wide variety of systems in both experimental [3–5] and theoretical studies [6–13]. Significant theoretical work was performed by Bogomolny [14] and Berry [15] (see also [16, 17]), which showed that the most stable of the unstable periodic orbits can give rise to enhanced probability along their trajectories in the energy-smoothed wavefunctions. However, this did not explain the appearance of scars in individual wavefunctions. Further progress came in [18] and [19], where a semiclassical scarring criterion was developed based on a resummed version of the Wigner function and the Fredholm method, respectively.

In this work we study the problem of phase-space structuring of quantum states, among them scarred states, from a slightly different point of view. We will first briefly introduce the scattering formalism for the quantization of billiards and explain the relation of the scattering

† Permanent address: Mathematics-Physics Department, University of Haifa at Oranim, Tivon 36006, Israel.

0305-4470/97/103613+22$19.50

matrix (or S-matrix) to the classical Poincaré map. We argue that S-matrix eigenvectors are physically relevant objects to consider, even when they do not correspond to quantized eigenstates. We introduce Wigner- and Husimi-like distributions on the Poincaré cell which allow us to relate the structure of quantum states to the underlying classical dynamics. At this stage we also introduce an observable $\mathcal{B}_{\mathrm{scar}}$ whose expectation value yields the degree of overlap of eigenvectors with a given set of phase-space points on the Poincaré cell, e.g. an unstable periodic orbit. After a rough categorization of S-matrix eigenvectors, we survey the structure of specific eigenvectors and present the relation to classical objects such as invariant tori and periodic points. Finally, we explain how S-matrix eigenphases evolve as functions of energy, and how this translates into the quantization of states. We conclude with a discussion of the main results and a few comments.

2. The scattering approach to quantization

We begin by introducing the scattering method of quantization introduced in [20] (a similar approach is Bogomolny's T-matrix method [21]; however, we will not directly refer to it here). For the sake of simplicity we restrict the discussion to autonomous systems with two degrees of freedom. Consider such a system, say two-dimensional billiard, which can be divided into two domains joined together along a line Γ. In the vicinity of Γ we decompose the wavefunction, $\Psi(\boldsymbol{r})$, into transverse normal modes,

$$\Psi(\boldsymbol{r}) = \sum_n \alpha_n \psi_n^{(2)}(\boldsymbol{r}) + \beta_n \psi_n^{(1)}(\boldsymbol{r}) \tag{1}$$

where $\psi_n^{(1,2)}(\boldsymbol{r})$ have the interpretation of propagating across Γ in different directions. For example, if Γ is a finite segment of the y-axis then the $\psi_n^{(1,2)}(\boldsymbol{r})$ would correspond to left- and right-going waveguide modes, respectively, while in the case where Γ denotes a circle $\psi_n^{(1,2)}(\boldsymbol{r})$ can be taken to be outgoing and incoming cylindrical waves.

After performing this decomposition, the problem has been transformed into the one of two back-to-back scattering systems. Let $\mathbf{S}^{(1)}$ and $\mathbf{S}^{(2)}$ denote the scattering matrices associated with the two systems, and let $\boldsymbol{\alpha}$ and $\boldsymbol{\beta}$ be vectors whose elements are the α_n, β_n, respectively. Then the scattering conditions can be written as

$$\boldsymbol{\beta} = \mathbf{S}^{(1)}\boldsymbol{\alpha} \qquad \boldsymbol{\alpha} = \mathbf{S}^{(2)}\boldsymbol{\beta}. \tag{2}$$

Consistency of these two conditions leads to a quantization condition which is in the form of a secular equation

$$\det(\mathbf{S} - \mathbf{I}) = 0 \qquad \mathbf{S} = \mathbf{S}^{(2)}\mathbf{S}^{(1)}. \tag{3}$$

Thus the system will have a quantized state whenever an eigenvalue of $\mathbf{S}$ is equal to unity. In this work we will refer to $\mathbf{S}$ as a scattering matrix as well, even though this usage is slightly unconventional. If the normal modes $\psi_n(\boldsymbol{r})$ are orthogonal and have an associated probability flux, j_n, across Γ, then from the principle of conservation of probability one can normalize $\mathbf{S}$ such that the subspace for which the j_n do not vanish is unitary. In the following we will assume this to be the case.

The operator $\mathbf{S}$ has a classical analogue in the Poincaré mapping. Let Γ be our Poincaré surface-of-section, and let us define the *Poincaré cell* to be the projection of the on-shell phase space onto this section. For simplicity we assume that the potential is constant in the vicinity of Γ, i.e. the section lies in free space, and that Γ is placed along a coordinate axis of a separable coordinate set, e.g. along a straight line or a circle. We also define the canonical phase-space coordinate pair (Q, P) in the vicinity of Γ, where Q is the coordinate

parallel to Γ. A point (Q, P) on the Poincaré cell now corresponds to a particle crossing Γ in a predefined transverse direction, say left to right, at parallel coordinate Q, and conjugate momentum P. The *Poincaré mapping* consists of mapping each point on the Poincaré cell to the point where the corresponding trajectory next intersects Γ with the proper orientation.

If the normal modes $\psi_n(\boldsymbol{r})$ correspond to the canonical quantization of, for example, the momentum P, there is a correspondence between the S-matrix and the Poincaré mapping, which is reflected in the fact that the elements of $\mathbf{S}$ can be represented semiclassically in terms of the trajectories participating in the Poincaré mapping [22–24]. However, a quantum analogue of the structures forming on the Poincaré cell is more problematic, since the quantum operator $\mathbf{S}$ does not operate in phase space but (in this example) in momentum space. Thus, while classically the current state of the Poincaré cell is defined by a two-dimensional real distribution, the quantum mechanical counterpart is the one-dimensional but complex coefficient vector $\boldsymbol{\alpha}$.

The use of the scattering formalism on the Poincaré cell to examine structuring of states was first proposed in [25], where the authors examined the structure of individual eigenstates on the Poincaré cell and worked out a semiclassical theory for these states in terms of composite periodic orbits. However, the Poincaré mapping operates in the time (or time-like) domain, while the study of individual eigenstates is by definition in the energy domain. It therefore seemed to us that perhaps the S-matrix itself deserves a closer look. In this work we use a formalism similar to the one introduced in [25] to examine the S-matrix, and in particular its eigenparameters, with and without the additional requirement of quantization.

To avoid cumbersome terminology, we limit the following discussion to the case where Γ denotes a circle of radius R_Γ centred around the origin. The natural axes to use on Γ in a scattering formulation are the impact parameter L and direction of propagation γ of a particle which intersects Γ on an in-bound trajectory. These coordinates are canonically conjugate via the *reduced* action [23, 26], which is the generating function for the mapping induced by the classical scattering process. Note that, since both γ and L are constants of motion for free propagation, the choice (γ, L) also ensures that our map is independent of R_Γ for a range of radii for which Γ is continually in free space. When quantizing it is natural to take the normal modes $\psi_n^{(1,2)}(\boldsymbol{r})$ to be given by outgoing and incoming cylindrical waves $\psi_n^{(1,2)}(\boldsymbol{r}) = \mathrm{i}^n \mathrm{H}_n^{(1,2)}(kr)\mathrm{e}^{\mathrm{i}n\phi}$, where $\mathrm{H}_n^{(1,2)}(\cdot)$ are the Hankel functions of the first and second kind, respectively, and k is the wavenumber. The index n signifies the quantized values of the angular momentum, $n = kL_n$. The S-matrix is then unitary without further normalization, and so its eigenvalues have the form $\lambda_j = \mathrm{e}^{\mathrm{i}\theta_j}$, and the quantization condition (3) is fulfilled whenever one of the eigenphases θ_j is equal to an integer multiple of 2π. We will also assume that the system in question is bounded by a circle of radius R, so that indices $n > kR$ correspond to classically forbidden motion. The infinite matrix $\mathbf{S}$ can then be truncated somewhere near $N = [kR]$, where $[\cdot]$ denotes the integer part, without losing too much of the dynamics.

The choice of Γ described above is (not accidentally) particularly suited to billiards, where the classical dynamics is free propagation between successive reflections off hard walls. The numerical examples in this work will be for the annular billiard introduced in [27], which is a system consisting of the space trapped between two non-concentric circles. We denote the radii of the outer and inner circles by R and a, respectively, and the distance between their centres by δ (we take the inner circle shifted to negative x values). As noted above, in such a system the Poincaré mapping is independent of R_Γ in the range $a + \delta < R_\Gamma < R$, and so we will assume that R_Γ satisfies this condition, and leave it unspecified.

The annular billiard can be quantized by requiring the wavefunction to vanish on the bounding circles (Dirichlet boundary conditions). In [28] the *S*-matrix for this system was shown to be

$$[\mathbf{S}]_{nm} = \mathrm{i}^{(n-m)} \frac{\mathrm{H}_n^{(1)}(kR)}{\mathrm{H}_n^{(2)}(kR)} \sum_{\ell=-\infty}^{\infty} J_{n-\ell}(k\delta) J_{m-\ell}(k\delta) \frac{\mathrm{H}_\ell^{(2)}(ka)}{\mathrm{H}_\ell^{(1)}(ka)}. \tag{4}$$

(We note that this form differs from the one given in [28] by the factor $\mathrm{i}^{(n-m)}$, which results from a slightly different definition of the $\psi_n^{(1,2)}(\boldsymbol{r})$.) In principle, $\mathbf{S}$ is infinite dimensional, but indices $|n| > N = [kR]$ correspond to classically forbidden motion (closed channels), and so we will take $\mathbf{S}$ to be a $(2N+1) \times (2N+1)$ matrix.

3. The Wigner–Poincaré distribution

In order to study the classical and quantum distributions on the Poincaré cell on the same footing, one can introduce what, in the absence of a better name, we call the Wigner–Poincaré distribution (WPD) [25], defined as follows. Let $\boldsymbol{\mathcal{A}}$ be some operator defined in angular momentum representation. The fact that the angular momentum is quantized introduces some needless complications, and so we will transform $\boldsymbol{\mathcal{A}}$ into its angular representation by means of a Fourier transform,

$$\hat{\boldsymbol{\mathcal{A}}} = \boldsymbol{\mathcal{F}} \boldsymbol{\mathcal{A}} \boldsymbol{\mathcal{F}}^\dagger \qquad \mathcal{F}_{\gamma,n} = \exp[-\mathrm{i}n\gamma]. \tag{5}$$

Then, the Wigner transform can be defined in the usual way as

$$\mathcal{A}_W(\gamma, n) = \frac{1}{2\pi} \int_0^{2\pi} \mathrm{d}\mu \hat{\mathcal{A}}_{\gamma - \frac{\mu}{2}, \gamma + \frac{\mu}{2}} \mathrm{e}^{-\mathrm{i}n\mu}. \tag{6}$$

Wigner functions are notorious for being very oscillatory, and so it is usually more useful to consider the Husimi transform, which is the minimal wavepacket smoothed version of the Wigner transform,

$$\mathcal{A}_H(\gamma, n) = \int_{-\infty}^{\infty} \mathrm{d}\nu \int_0^{2\pi} \mathrm{d}\phi \, \mathcal{A}_W(\phi, \nu) \exp\left[-\frac{(\gamma - \phi)^2}{2\Delta\gamma^2} - \frac{(n-\nu)^2 \Delta\gamma^2}{2} \right] \tag{7}$$

where $\Delta\gamma^2$ is a parameter determining the shape of the smoothing minimal uncertainty wavepacket. We will choose $\Delta\gamma^2 = 4/k$.

We now take $\boldsymbol{\mathcal{A}}$ to be the 'density operator' corresponding to some coefficient vector $\boldsymbol{\alpha}$, $\boldsymbol{\mathcal{A}} = \boldsymbol{\alpha}\boldsymbol{\alpha}^\dagger$. The resulting Wigner- and Husimi-transformed objects we call the WPD, $\rho_{\boldsymbol{\alpha}}^{\mathrm{W}}$, and Husimi–Poincaré distribution (HPD), $\rho_{\boldsymbol{\alpha}}^{\mathrm{H}}$. Both quantities are real, and the WPD satisfies the usual projection conditions

$$\sum_{n=-\infty}^{\infty} \rho_{\boldsymbol{\alpha}}^{\mathrm{W}}(\gamma, n) = |\hat{\alpha}_\gamma|^2 \tag{8a}$$

$$\frac{1}{2\pi} \int_0^{2\pi} \mathrm{d}\gamma \, \rho_{\boldsymbol{\alpha}}^{\mathrm{W}}(\gamma, n) = |\alpha_n|^2 \tag{8b}$$

for integer n. Thus both quantities are normalized to unity (if $\|\boldsymbol{\alpha}\| = 1$, which we will always assume). Moreover, $\rho_{\boldsymbol{\alpha}}^{\mathrm{H}}$ is positive semi-definite, and so can be given the interpretation of a distribution over the Poincaré cell. It is this distribution which we would like to correlate to classical phase-space structures.

For completeness it should be mentioned that, except possibly at quantized energies, in most cases there is no clear relation between the WPD and the projection of a Wigner transformed wavefunction (even a time-dependent one) onto the Poincaré surface-of-section.

This is because iterations of $\mathbf{S}$ are not quite equivalent to time, since different points on the Poincaré cell will return to it after different intervals of time. For a system such as the annular billiard the return time is bounded, and so the difference between iterations and time is not very great. However, in the presence of chaotic scattering (see [30]) the return times may be infinite even for one S-matrix iteration.

Up till now we have kept the coefficient vectors $\boldsymbol{\alpha}$ arbitrary. However, in order to be meaningful these vectors must be in some way related to the system at hand. In [31] we use the HPD to follow the time evolution in phase space of a quantum system in much the same way that one would follow the time evolution of a Poincaré map. The quantities we focus on in this work are vectors $\boldsymbol{\alpha}^{(j)}$ which are *eigenvectors* of the scattering matrix $\mathbf{S}$, with an associated eigenphase θ_j. An eigenvector of $\mathbf{S}$ does not in general correspond to an eigenstate of the system, since for that θ_j would have to be an integer multiple of 2π. However, in the time domain (or more precisely, the time-like domain defined by repeated iterations of $\mathbf{S}$) an eigenvector corresponds to a phase-space distribution $\rho_{\boldsymbol{\alpha}}^{\mathrm{H}}$ that remains invariant under iteration of $\mathbf{S}$, $\rho_{\boldsymbol{\alpha}^{(j)}}^{\mathrm{H}} = \rho_{\mathbf{S}\boldsymbol{\alpha}^{(j)}}^{\mathrm{H}} \equiv \rho_j^{\mathrm{H}}$, since the HPD $\rho_{\boldsymbol{\alpha}}^{\mathrm{H}}$ is insensitive to the multiplication of $\boldsymbol{\alpha}$ with a phase.

We see that at *any* energy the system supports a set of $2N+1$ stationary phase-space distributions ρ_j^{H}. The time domain therefore affords a much richer environment for study than the energy domain, where only one wavefunction at a time is available for study, and that only on a discrete set of energies. The two descriptions intersect at the quantized energies, where one of the ρ_j^{H} represents the current eigenstate. This does not mean, however, that the other eigenvectors do not contain information about the system. This approach also allows us to disentangle the two issues of energy quantization and wavefunction structure, and treat them separately.

Finally, it is instructive to develop the expression (7) explicitly for the density operator $\boldsymbol{\mathcal{A}} = \boldsymbol{\alpha}\boldsymbol{\alpha}^{\dagger}$. Inserting (5) and (6) into (7), expanding and performing the integrations gives

$$\rho_{\boldsymbol{\alpha}}^{\mathrm{H}}(\gamma, n) = \sum_{\ell\ell'} \alpha_\ell \alpha_{\ell'}^* \exp\left\{ \frac{-\Delta\gamma^2}{2} \left[\left(n - \frac{\ell+\ell'}{2} \right)^2 + (\ell-\ell')^2 \right] - \mathrm{i}\gamma(\ell-\ell') \right\}. \tag{9}$$

From (9) one can see that $\rho_{\boldsymbol{\alpha}}^{\mathrm{H}}(\gamma, n)$ is a *local* property of the vector $\boldsymbol{\alpha}$, in the sense that it depends only on the components α_ℓ for which ℓ is within a few $\Delta\gamma^{-1}$ of n. A similar property holds in the angular representation.

Suppose we now want to measure the amount of overlap of $\rho_{\boldsymbol{\alpha}}^{\mathrm{H}}$ with a set of points $\{\gamma_j, L_j\}_{j=1}^{T}$ on the Poincaré cell. In the sequel we will use such an overlap to look for vectors which are localized (scarred) by specific periodic orbits. A natural definition of the overlap is

$$\mathcal{B}(\boldsymbol{\alpha}) = \sum_{j=1}^{T} \rho_{\boldsymbol{\alpha}}^{\mathrm{H}}(\gamma_j, kL_j). \tag{10}$$

Then, from (9) we can define the observable $\boldsymbol{\mathcal{B}}_{\mathrm{scar}}$ by

$$[\boldsymbol{\mathcal{B}}_{\mathrm{scar}}]_{\ell\ell'} = \sum_{j=1}^{T} \exp\left\{ \frac{-\Delta\gamma^2}{2} \left[\left(kL_j - \frac{\ell+\ell'}{2} \right)^2 + (\ell-\ell')^2 \right] - \mathrm{i}\gamma_j(\ell-\ell') \right\}. \tag{11}$$

Comparing with (9) we see that the overlap is simply given by the expectation value $\mathcal{B}(\boldsymbol{\alpha}) = \boldsymbol{\alpha}^{\dagger}\boldsymbol{\mathcal{B}}_{\mathrm{scar}}\boldsymbol{\alpha}$. This procedure is similar in spirit to the scarring quantity for the Husimi distributions of quantized levels proposed in [9]. Furthermore, this scarring observable is more powerful than, for example, the one proposed in [25], since it operates in phase space and so can unambiguously focus on a desired classical trajectory. It is also easy and fast to implement numerically. We will give examples of the use of this observable later on.

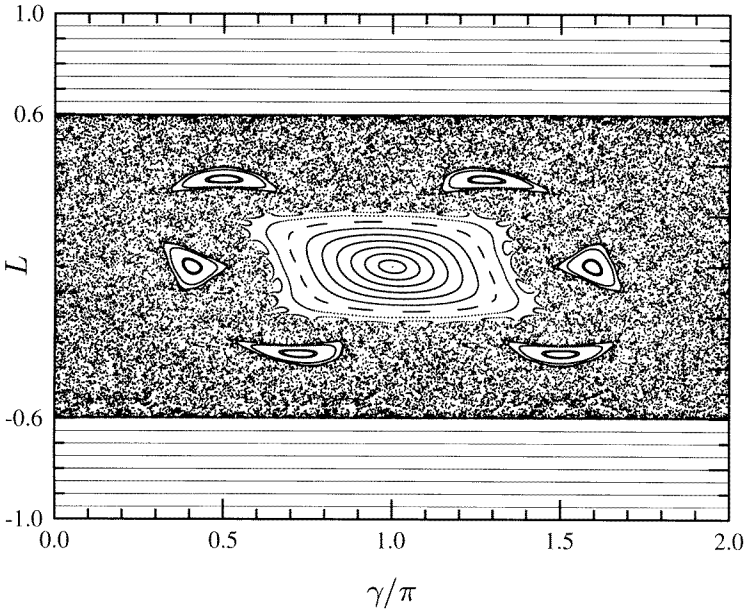

Figure 1. The Poincaré surface-of-section map for the annular billiard, for parameter values $R = 1$, $a = 0.4$ and $\delta = 0.2$.

4. Eigenstructures of the annular billiard

In this section we examine the structures that one can find among the eigenvectors of **S** for the annular billiard (see (4)). In order to do this, let us first describe the classical structures one encounters in the Poincaré map.

Figure 1 shows a Poincaré map for the annular billiard, at parameters $a = 0.4$, $\delta = 0.2$, $R = 1$. For values of the impact parameter $L > a + \delta$ a trajectory will never impact the inner circle. L is then a constant of motion, which means that motion is regular and will project onto the Poincaré cell along straight, horizontal lines. This is just the motion that one would expect in the absence of the inner circle.

For lower values of the impact parameter, a trajectory will at some stage hit the inner circle, and since the circles are not concentric, motion will no longer be integrable. This can give rise to the whole range of phenomena associated with non-integrable systems with a mixed-phase space: regular islands and island chains, chaotic regions, partial transport barriers (cantori) and the like. In figure 1 we can see a large regular island at the centre, encapsulating an elliptic fixed point which corresponds to the periodic orbit which bounces between the two circles along the x-axis on the right-hand side of the billiard. Its sister orbit, which bounces along the x-axis on the left-hand side of the billiard, is unstable and lies at the heart of the chaotic sea. In addition, we see a regular island chain surrounding the centre island, which in fact comprises a *single* regular region encapsulating a period-6 elliptic periodic orbit. Finally, near the boundary between the integrable and non-integrable regions there are several smaller regular island chains.

We see that the annular billiard displays the whole range of structures one might expect to find in a two-degree-of-freedom system with mixed dynamics. One then asks how this manifests in the structure of the eigenvectors of its S-matrix. Following the examples of [32, 33], we first obtain a rough classification of eigenvectors. Let us define for an

eigenvector $\boldsymbol{\alpha}^{(j)}$ the following quantities:

$$\mathcal{N}_j = \left[\sum_n n^2 |\alpha_n^{(j)}|^2 \right]^{1/2} \qquad \mathcal{S}_j = -\sum_n |\alpha_n^{(j)}|^2 \log |\alpha_n^{(j)}|^2. \tag{12}$$

These quantities can be interpreted as the root-mean-square angular momentum and the Shannon entropy of $\boldsymbol{\alpha}^{(j)}$, respectively. It is instructive to briefly consider two limiting cases. Each member of a regular high-angular-momentum doublet peaked at $\pm n$ will have $\mathcal{N}_j \approx n$ and $\mathcal{S}_j \approx \log 2$. On the other hand, chaotic eigenvectors will have $\mathcal{N}_j$ somewhere between 0 and $k(a+\delta)$. To estimate their entropy, we assume that their elements are Porter–Thomas distributed [34] over some number, N_γ, of components,

$$\mathrm{P}(x = |\alpha_n|^2) = \left(\frac{N_\gamma}{2\pi x}\right)^{1/2} \exp\left(-\frac{x N_\gamma}{2}\right)$$

and zero otherwise. The mean entropy of such vectors can be calculated from

$$\begin{aligned} \langle \mathcal{S}_j \rangle &= \frac{N_\gamma^{3/2}}{2\pi} \int_0^\infty \mathrm{d}x\, x^{1/2} \log x \mathrm{e}^{-xN_\gamma/2} \\ &= \log(N_\gamma) + \log 2 - 2 + \gamma_E \approx \log(0.48 N_\gamma) \end{aligned} \tag{13}$$

where γ_E denotes Euler's constant. This can be used to scale out the energy dependence of the entropy of chaotic vectors: since N_γ scales roughly like $N_\gamma \propto k$, we can expect $\langle \mathcal{S}_j \rangle - \log(0.48k) \approx \log(N_\gamma/k)$ to be independent of k for chaotic eigenvectors. Consequently, we will use scaled axes and plot $\tilde{\mathcal{N}}_j = \mathcal{N}_j/k$ as a function of $\tilde{\mathcal{S}}_j = \mathcal{S}_j - \log(0.48k)$.

We present in figure 2 three $\tilde{\mathcal{N}}_j - \tilde{\mathcal{S}}_j$ diagrams of S-matrix eigenvectors at different wavenumbers $k = 100$, 200 and 600. The data points follow a relatively narrow distribution. Starting from the upper left corner, we find regular, high angular momentum doublets at $\tilde{\mathcal{N}}_j \gtrsim 0.6$ and $\tilde{\mathcal{S}}_j \approx \log(4/k)$, then see a smooth transition regime of edge eigenvectors towards smaller $\tilde{\mathcal{N}}_j$ and higher $\tilde{\mathcal{S}}_j$ until the entropy achieves its maximal value in the range of $-0.5 \leqslant \tilde{\mathcal{S}}_j \leqslant 0$. This is mainly the domain of vectors supported by the chaotic layer. Towards lower $\tilde{\mathcal{N}}_j$, we again find regular vectors: a distinct strip of data points around $\tilde{\mathcal{N}}_j \approx 0.28$ that corresponds to regular vectors supported by the centre satellite islands (towards lower entropy) and their sticking region (towards higher entropy), and a line of decreasing $\tilde{\mathcal{S}}_j$ and $\tilde{\mathcal{N}}_j$ (down $\tilde{\mathcal{S}}_j \approx -2$ and $\tilde{\mathcal{S}}_j \approx 0$) that corresponds to vectors supported by the centre regular island.

A word of caution is in place here: the value obtained for $\mathcal{S}_j$ in (12) depends on the representation chosen for the eigenvectors. This probes only *one* axis in phase space and does not necessarily allow conclusions on the Poincaré cell structure of the quantum state. For example, for a state localized at a certain angular momentum value, (12) gives a low entropy, whereas for a state localized at a certain angle, the broad distribution in angular momentum will lead to a high value of $\mathcal{S}_j$.

As the energy is increased, the data points 'condense' onto the line just described. We see that for chaotic vectors, $\langle \tilde{\mathcal{S}}_j \rangle$ is roughly constant. This can be used to extract $N_\gamma/k \approx 0.9$ as a measure of the classical phase-space volume occupied by chaotic states. As k increases, N_γ/k decreases slightly, which might be attributed to the more rapid decay of overlaps away from the supporting phase-space region at higher energies. Anyhow, it must be emphasized that the scaling of $\langle \tilde{\mathcal{S}}_j \rangle$ does not serve as a conclusive argument for the Porter–Thomas distribution of chaotic eigenvectors: many other distributions yield similar scaling laws of $\langle \tilde{\mathcal{S}}_j \rangle$ with $\log k$, and a distinction cannot be made from the numerical data

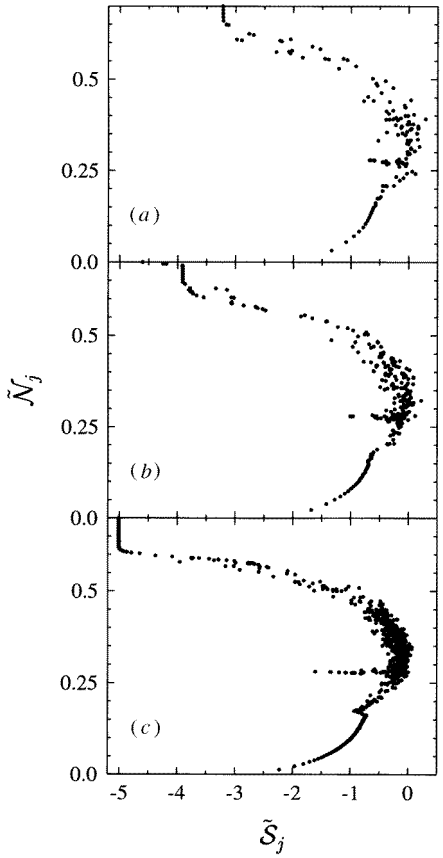

Figure 2. A plot of the root-mean-square angular momentum, $\mathcal{N}$, versus the entropy, $\mathcal{S}$, of eigenvectors of the annular billiard for parameter values $R = 1$, $a = 0.4$ and $\delta = 0.2$, and at energies $k = 100$ (a), $k = 200$ (b) and $k = 600$ (c). The axes are scaled to remove the dominant energy dependence (see text).

presented. Indeed, in the present system it is our experience that a large proportion of the irregular states possess an HPD which is highly localized around classical structures, and so are quite far from the Porter–Thomas ansatz in phase space. However, we can tentatively conclude from the scaling results that the structure of all but the regular eigenvectors is based on some underlying classical partition of phase space.

The $\tilde{\mathcal{N}}_j$–$\tilde{\mathcal{S}}_j$ diagram provides us with a global overview of the properties of eigenvectors. We are, however, more interested in the fine structure of *individual* eigenvectors. In the rest of this section we investigate this point by examining the phase-space structure of eigenvectors by means of their HPD. Almost all of the eigenvectors displayed in this section are evaluated at $k = 600$, which one should note is not an eigenenergy of the annular billiard.

Let us start by examining the effects of the regular phase-space regions. In figures 3(a)–(c) we show several HPDs, overlaid by a plot of the positions of the sizeable classical stable islands that exist in the Poincaré map. One can see that the specific HPDs shown all reside on or in a classically stable region—either the main stable island in the middle, its primary satellite islands, or in the near-integrable region of high angular momentum $n > k(a + \delta)$. Note that, as has been observed before [35, 36], quantum regularity extends

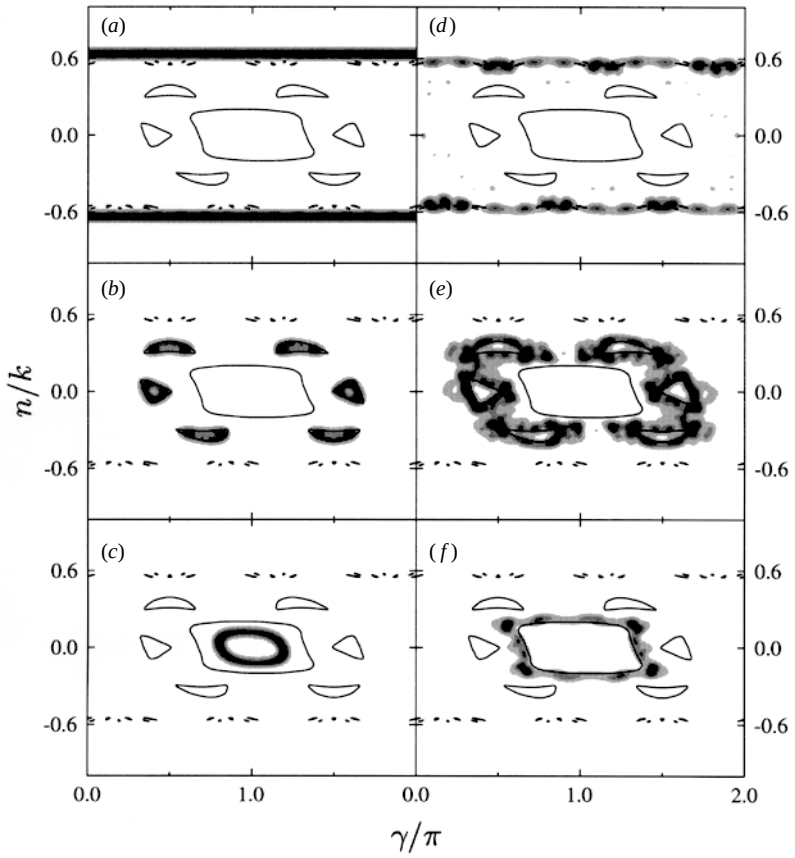

Figure 3. The HPD of several regular or near-regular eigenvectors at $k = 600$. The full lines depict the sizeable classical regular islands in the Poincaré surface-of-section. (*a*), (*b*) and (*c*) show eigenvectors which are supported by classically regular phase-space regions. (*d*), (*e*) and (*f*) show eigenvectors which are supported by the 'sticking' regions surrounding classically stable islands.

further into phase space than does classical stability. This is attributed to the relatively stable classical motion in the transition layer between regular and chaotic phase-space regions that gives rise to staying times much larger than the mean level density, which in turn leads to quantization of states on this phase-space region. In figures 3(*d*)–(*f*) we show several eigenvectors which seem to be supported by the interface region between the regular and chaotic regions. In particular, the boundary regions $|n| \lesssim k(a + \delta)$ support a series of regular-looking eigenvectors which extend well into the classically chaotic regions. These so-called edge states were of critical importance to the understanding of 'chaos-assisted tunnelling' in this system, i.e. tunnelling between pairs of regular states of high-angular momentum via the chaotic sea [28].

Next, let us examine some 'chaotic' eigenvectors, i.e. those whose HPD has its support mainly in the classically chaotic region. It seems that a sizeable number of such eigenvectors are structured, and several of these are displayed in figure 4. On the right side of the figure we show some chaotic HPDs, and on the left side the configuration-space representation of the scarring periodic orbits, of period-4, period-6 and period-8. The surface-of-section

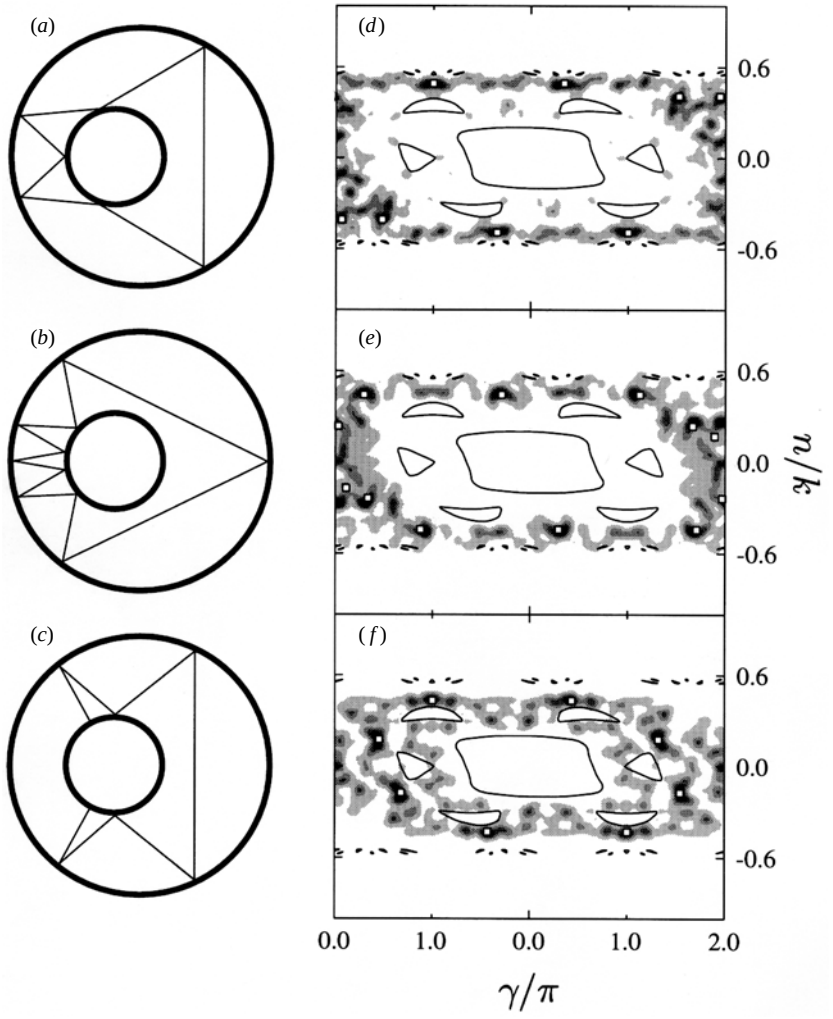

Figure 4. The HPD of several scarred 'chaotic' eigenvectors at $k = 600$, together with a configuration space plot of the scarring unstable periodic orbit. The full lines depict the sizeable classical regular islands in the Poincaré surface-of-section. The projections of the periodic orbits (and their time-reversed partners) onto the Poincaré cell are shown as small white squares.

representation of the orbits is also overlaid on top of the HPDs, in the form of small open squares. Note that, unless the orbit is self-retracing, each plot represents *two* orbits, since each orbit has a time-reversed partner. The fit is quite distinctive (keeping in mind that the x-axis is actually a periodic angular coordinate). It should again be mentioned that all the above distributions are calculated for the same system and at the same energy $k = 600$.

In [10] it was suggested that specific unstable periodic orbits can support a whole family of scarred states. A demonstration that this also applies to eigenvectors is shown in figure 5. The full curves in the figure trace the stable and unstable manifolds of the hyperbolic fixed point, and one can see a remarkable structure build up along these manifolds. Figure 5(a) shows the 'fundamental' scarred eigenvector. It is heavily localized on top of the fixed point, but local maxima of probability also appear along the stable/unstable manifolds, and most

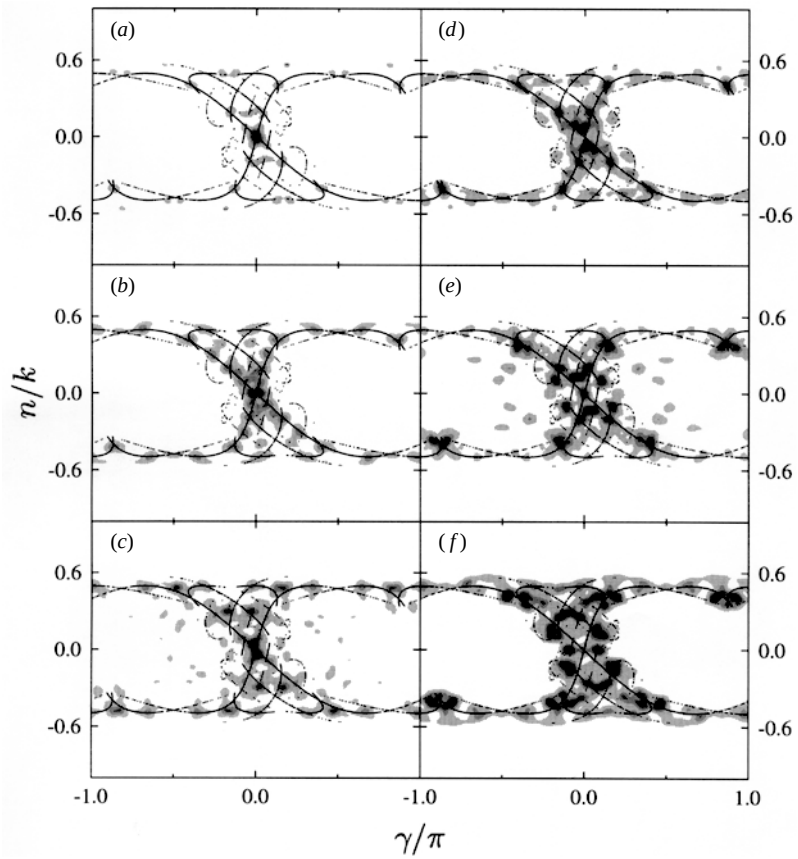

Figure 5. The HPD at $k = 600$ of several eigenvectors which are scarred by the unstable fixed point. The lines trace the stable and unstable manifolds of the fixed point. Note that the γ-axis is shifted by π relative to the previous plots.

prominently at the homoclinic intersections of the manifolds. Figure 5(b) shows another scarred eigenvector which displays much more probability at the homoclinic intersections. In figure 5(c) the main peak at the fixed point begins to split vertically, a process which continues in figures 5(d) and (e). Finally, comparing figures 5(d)–(f) we see that one can get the maxima at the homoclinic intersections to successively split up as well. This set of examples is strongly reminiscent of a set of EBK-quantized states with two approximate internal 'quantum numbers'. We note that, while scars have been observed before to extend themselves along the stable and unstable manifolds of periodic orbits (see e.g. [6, 10]), in this case we observe scars which extend along the manifolds for the entire width of the system, not just in the close vicinity of the scarring orbit. Additionally, even though some indications of this effect have been seen before [9], this is the first time to our knowledge that the importance of the homoclinic intersections have been demonstrated in such a clear fashion.

For completeness, we also check the correspondence between specific HPDs and quantized wavefunctions. In figure 6(a) we show a grey-scale plot of a quantized wavefunction at $k = 86.492$ in configuration space. One can see that this particular wavefunction is structured, although it is not immediately obvious by what—there is a

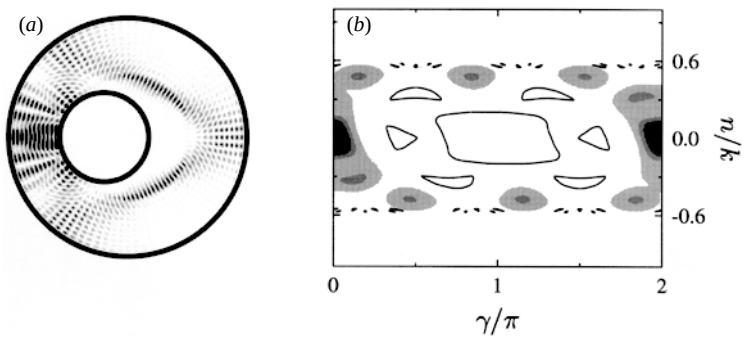

Figure 6. A quantized wavefunction (*a*) and corresponding HPD (*b*) at $k = 86.492$. The full lines in (*b*) depict the sizeable classical regular islands in the Poincaré surface-of-section.

pile-up of probability along the shortest unstable periodic orbit, but one can also discern a triangular structure along the left-hand side of the billiard which might or might not have something to do with a classical trajectory. This ambiguity is removed by examining the corresponding HPD, which can be seen in figure 6(*b*). Most of the probability is indeed localized around the hyperbolic fixed point ($\gamma = 0, L = 0$), and the triangular structures seen in the wavefunction can be attributed to the contributions of the orbit's primary and secondary homoclinic intersections.

5. Evolution of eigenvectors and eigenphases

The $\tilde{\mathcal{N}}_j$–$\tilde{\mathcal{S}}_j$ diagrams presented in the previous section suggest that the classification of states by the classical nature of their supporting phase-space regions is more or less followed. A similar observation concerning energy-quantized eigenfunctions has been made in [13]. However, we would like to go a step further, and conjecture that at least those eigenvectors which are shaped by an underlying classical structure (not just an entire phase-space region) also retain their identity over a significant range in energy. For example, an eigenvector which is scarred by a given periodic orbit will evolve in energy to a very similar-looking eigenvector, whose HPD is scarred by the same periodic orbit. Thus the picture that we suggest is that at any (sufficiently high) energy the S-matrix supports a set of structured (regular, inner-island, scarred, etc.) eigenvectors, which retain their identity across an energy range which is much larger than the mean level spacing (note that we are not claiming that all eigenvectors are structured). As the energy is increased, the eigenphases associated with those eigenvectors will 'rotate' around the unit circle with some 'velocity'. Whenever one of these eigenphases passes through an integer multiple of 2π the system quantizes, and the structure of the quantized eigenfunction is determined by the identity of the quantizing eigenvector. If this picture is correct, it means that phase-space structure and quantization are two distinct issues, which should be dealt with separately. In this section we will explore this possibility by numerically investigating the energy dependence of the eigenparameters of the S-matrix derived for the annular billiard.

Let us first determine the average energy dependence of all of the eigenphases. This mean can be obtained from rather general considerations, first applied in [20]. The mean level density in a billiard can be approximated by the leading order of the Weyl formula [37], $\langle d(k) \rangle \approx kA/2\pi$, where A is the area of the billiard. Let us define the 'eigenphase velocity' $\tau_\ell = \partial\theta_\ell/\partial k$. Since $\tau_\ell > 0$ [38], the rate at which θ_ℓ crosses a multiple of 2π is

$\tau_\ell/2\pi$. Comparing this with the Weyl formula gives

$$\sum_\ell \tau_\ell \approx kA. \tag{14}$$

For the annular billiard the number of contributing channels is $2kR$, and the area is $A = \pi(R^2 - a^2)$. Thus the mean velocity is

$$\langle \tau_\ell \rangle \approx \frac{\pi(R^2 - a^2)}{2R}. \tag{15}$$

Note that $\langle \tau_\ell \rangle$ is thereby determined by a purely classical quantity.

Equation 15 gives the mean behaviour of the eigenphases. However, we are more interested in the evolution of *individual* eigenphases and eigenvectors. As always, we begin with the eigenphases belonging to eigenvectors of high angular momentum. For $n > k(a + \delta)$ the S-matrix is roughly diagonal, and so the associated eigenvectors are well approximated by combinations of angular momentum states $|\pm n\rangle$. The corresponding eigenphase is approximately

$$e^{i\theta_n} \approx -\frac{H_n^{(1)}(kR)}{H_n^{(2)}(kR)} \approx \exp\left[-2ikR(\sin Q - Q\cos Q) - i\frac{\pi}{2}\right] \qquad Q = \arccos\left(\frac{n}{kR}\right) \tag{16}$$

where the second equality results from the Debye approximation for $n \sim k \gg 1$ [39], which is equivalent in this case to the semiclassical approximation. Differentiating the phase with respect to k then yields

$$\tau_n = \frac{\partial\theta_n}{\partial k} \approx 2\sqrt{R^2 - \left(\frac{n}{k}\right)^2}. \tag{17}$$

This quantity can be given a simple classical interpretation, as follows. Consider a straight line with impact parameter n/k, which is just the classical impact parameter associated with the angular momentum states $|\pm n\rangle$. Then, τ_n is given by the distance between the two intersections of this line with the R circle. In other words, τ_n is given by the path length of the appropriate trajectory between two consecutive intersections with the Poincaré surface-of-section.

The regular high angular momentum states are easily identifiable by virtue of being almost exclusively localized at angular momenta $\pm n$, and interact only weakly with other states. Consequently, both their structure and their velocity are straightforward to define. This is not necessarily the case for the irregular eigenvectors, and poses the question of how to track an eigenvector across a sizeable range in energy. One way to do that is to diagonalize $\mathbf{S}$ on a set of closely spaced energy values, and to track the eigenphases. However, this method will break down at an avoided crossing between the tracked eigenphase and another one, since in the vicinity of the avoided crossing the two states mix, and then part ways after having interchanged their identity. Thus the energy derivatives of the eigenphases are *not equivalent* to the 'velocity' associated with a particular structured eigenvector. Rather, one has to track the eigenvector across many avoided crossings to obtain a meaningful velocity.

Another potential complication is that specific classical structures may support more than one eigenvector at any given energy. We can therefore attempt to label individual eigenvectors by the classical structure which supports them, plus one or more 'quantum numbers' which distinguish between different excitations which might belong to the structure. For example, a single regular island in phase space might be large enough to support a whole set of states, which can be ordered into a fundamental 'ground state' and set of excitations on the island. Similarly, an unstable periodic orbit might support one scarred eigenvector, or if it is stable enough it might support more than one (see also [10]).

The thesis we are advancing in this work is that a set of quantum phase-space structures exist which are stable in the sense that eigenvectors with a specific HPD can be found over a large range in energy. We therefore suppose that the difficulties detailed above can be overcome by carefully examining the HPDs of the eigenvectors, and let us limit the discussion to eigenvectors whose HPD is dominated by one specific (stable or unstable) periodic orbit. A natural classical parameter is then the length of the orbit. This parameter also appears in suggested EBK-like criteria for quantization of scarred states [9, 18, 25]. In the following we examine the relation between the orbit length and the eigenphase velocity for structured eigenvectors in the annular billiard.

Let us first consider the central stable island. The primary classical structure associated with this island is the stable fixed point at ($\gamma = \pi, L = 0$), which corresponds in configuration space to a periodic orbit of length $\lambda_s = 2(1 - a + \delta) = 1.6$ which bounces between the two circles along the x-axis on the right-hand side of the billiard. Note that λ_s is significantly larger than the mean eigenphase velocity $\langle\tau\rangle = 1.32$. The prediction is, therefore, that over a wide range in energy one can find an eigenvector which is the 'fundamental' of the stable island, in the sense that its HPD is localized at the fixed point itself, and that the associated eigenphase increases linearly with the energy with a rate given by λ_s.

The annular billiard also supports an unstable fixed point, corresponding in configuration space to a periodic orbit of length $\lambda_u = 2(1 - a - \delta) = 0.8$ which bounces between the two circles along the x-axis on the left-hand side of the billiard. In this case λ_u is significantly *smaller* than the mean velocity. As in the case of the regular island, more than one eigenvector is scarred by this periodic orbit (see figure 5), and so we examine only the 'fundamental' excitation, i.e. that whose HPD is localized most strongly on the fixed point.

The predictions given above are tested in figure 7. Figure 7(a) shows a configuration space plot of the periodic orbits which correspond to the stable (broken curve) and unstable (full curve) fixed points of the Poincaré mapping. Figure 7(b) displays the eigenphases associated with eigenvectors whose HPD are most strongly localized on the stable (squares) and unstable (circles) fixed points, over the range $150 \leqslant k \leqslant 160$, and figures 7($c$) and ($d$) show the HPDs of such eigenvectors. The HPDs are evaluated at $k = 160$, but do not change their form over the entire displayed energy range. Note in figure 7(d) the now-familiar secondary probability maxima at the homoclinic intersections of the unstable fixed point.

One can see in figure 7(b) that the eigenphases follow a linear increase with k. For comparison, we have also overlaid straight lines with the predicted slopes of λ_s and λ_u. In the case of the stable fixed point, all of the eigenphases lie exactly on the predicted line. In the case of the unstable fixed point, we see that the mean slope is well given by λ_u, but that the local slopes may be bigger. The reason for this is the following. Since λ_u is significantly smaller than $\langle\tau\rangle$, there are numerous avoided crossings between the scarred eigenvector we are tracking and other eigenvectors. Because the unstable fixed point resides in a chaotic part of the classical phase space, these avoided crossings are not small, and give rise to local slopes which are larger than those obtained by tracking the scarred eigenvector across a large energy range. In contrast, the stable regular island comprises a near-integrable and almost isolated subsystem. Its eigenvectors consequently do not 'interact' with each other or with the chaotic eigenvectors, and one can neglect the effects of avoided crossings.

We see that one can associate the fixed points of the mapping with a set of structured eigenvectors, whose eigenphases increase linearly with k with a velocity given by the length λ of the associated classical orbit. A consequence of this is that a structured quantized state corresponding to these structured eigenvectors will recur at regular energy intervals of

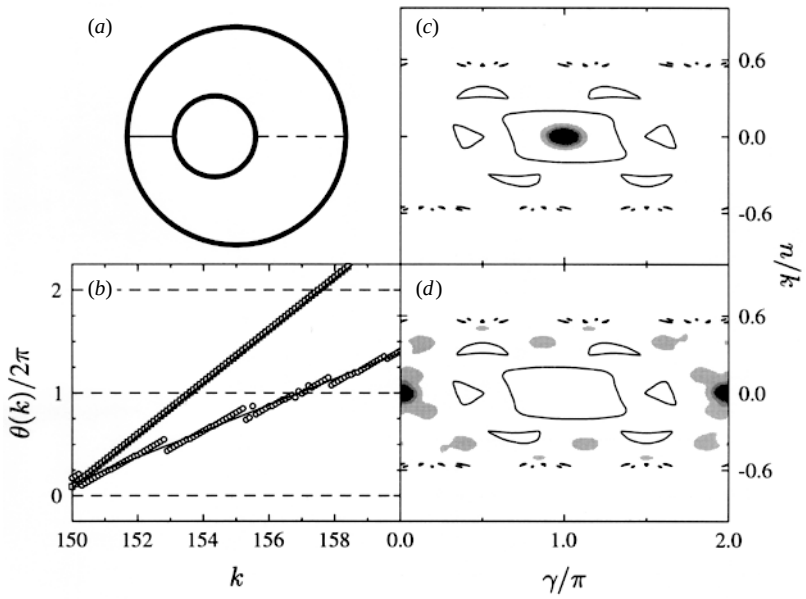

Figure 7. The energy dependence of the eigenphases associated with eigenvectors which are scarred by the fixed points of the Poincaré mapping for the annular billiard. (*a*) The configuration-space plot of the stable (broken line) and unstable (full line) periodic orbits corresponding to the fixed points of the Poincaré mapping. (*b*) The eigenphases associated with scars on the stable (squares) and unstable (circles) fixed point. The full curves depict slopes of $\lambda_s = 1.6$ and $\lambda_u = 0.8$, and the broken curves mark integer multiples of 2π. (*c*) The HPD of a stable-fixed-point eigenvector at $k = 160$. (*d*) The HPD of an unstable-fixed-point eigenvector at $k = 160$.

$\Delta k = 1/\lambda$. This is consistent with an approximate EBK quantization along the orbit which has been suggested and observed in [7, 9, 18, 25].

The examples given above were for periodic orbits which are fixed points of the Poincaré mapping. The situation becomes more involved for periodic orbits with a Poincaré-map period $T > 1$, since then we encounter a seeming paradox. On the one hand, the mean eigenphase velocity is given by (15), which is also roughly the mean length of an arbitrary trajectory between two successive intersections with the Poincaré surface-of-section. On the other hand, the natural scale to associate with a given periodic orbit is its *total* length, which is of the order of $\sim T\langle\tau\rangle$, and for $T \gg 1$ is much larger than the mean behaviour. This apparent incompatibility resolves itself in a somewhat surprising manner, as we shall see below.

In order to track specific structured eigenvectors we applied the scarring observable $\mathcal{B}_{\rm scar}$ (see equation (11)) to the eigenvectors of $\mathbf{S}$ over an entire range in energy, and selected the eigenvectors with the highest expectation value for $\mathcal{B}_{\rm scar}$ for the desired periodic orbits. In figure 8 we display the eigenphases and HPD of the first few eigenvectors which are most scarred by periodic orbits of period 4 ((*g*) and (*b*) showing the nine most scarred eigenvectors), period 5 ((*c*) and (*d*) showing eight most scarred eigenvectors) and period 6 ((*e*) and (*f*) showing six most scarred eigenvectors), over the range $150 \leqslant k \leqslant 160$. The period-4 and period-5 orbits are unstable (the period-5 orbit is the one displayed in figure 10(*a*)), while the period-6 orbit is stable and lies at the heart of the satellite regular

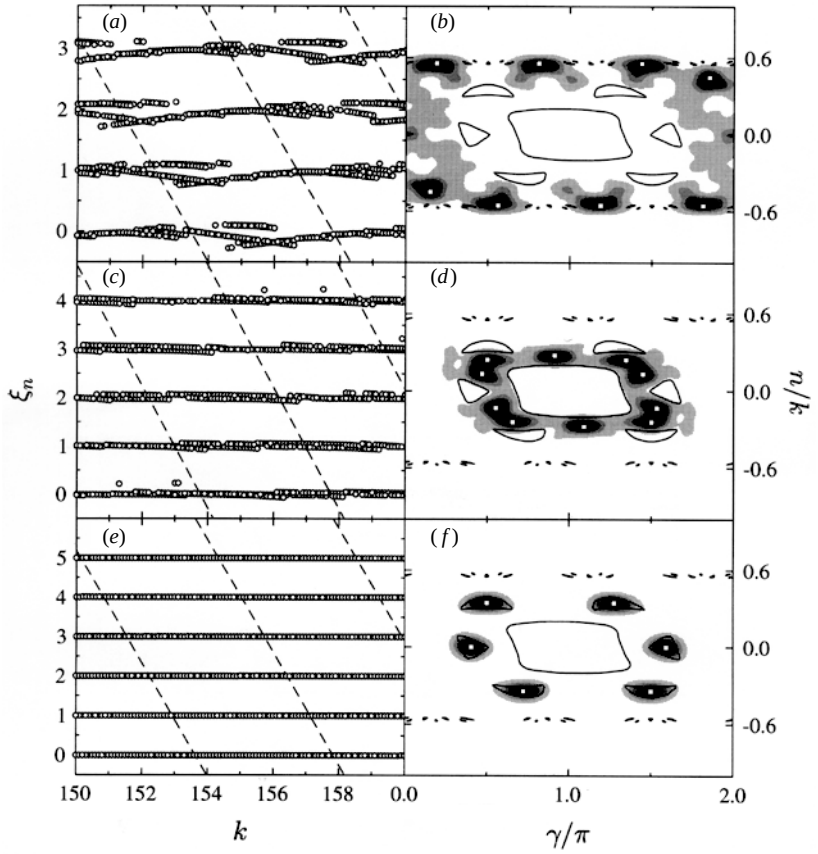

Figure 8. (*a*), (*c*) and (*e*) The rescaled eigenphase, ξ_n (see (18)), versus the wavenumber, k, for eigenvectors which have maximal overlap with a period-4 unstable periodic orbit (*a*), a period-5 unstable periodic orbit (*c*), and a period-6 stable periodic orbit (*e*). The broken curves represent unrescaled phases which are integer multiples of 2π. (*b*), (*d*) and (*f*) The HPD of scarred eigenvectors at $k = 160$ for the period-4 (*b*), period-5 (*d*) and period-6 (*f*) periodic orbits. The open squares represent the intersections of the orbit and its time inverse with the Poincaré cell, while the full lines depict the sizeable classical regular islands.

islands in the Poincaré map. The quantity which is actually plotted in the phase plots is

$$\xi_n = \frac{\theta_n - k\lambda/T}{2\pi/T} + \xi_0 \tag{18}$$

where ξ_0 is an arbitrary phase shift which is included for convenience. ξ_n removes from θ_n an increasing slope of λ/T, and rescales so that the phase is displayed in multiples of $2\pi/T$. Remarkably, for the three families of scarred eigenvectors displayed in figure 8, ξ_n falls almost exactly on the integers. Since the removed slopes are of the order of ~ 1.5 (see the broken curves), the figure shows that the classically obtained slopes are accurate to within 1% or less.

The resolution is therefore the following. Rather than a single eigenvector whose eigenphase evolves with 'velocity' λ, the S-matrix supports $\sim T$ (or $\sim 2T$, see below) eigenvectors structured by the same periodic orbit, each with an eigenphase velocity of λ/T. Thus, on the one hand, individual velocities do not deviate too much from the mean

$\langle \tau_\ell \rangle$ as given in equation (15), but, on the other hand, quantization will yield structured eigenstates with spacings of $\Delta k = 2\pi/\lambda$, as expected from EBK-like considerations. However, successively structured eigenstates do not in some sense represent the 'same' scar, since smoothly tracking a given structured eigenvector yields quantized structured eigenstates with a wavenumber separation of $2\pi T/\lambda$.

A careful look reveals some differences between the behaviours of the eigenvectors which are scarred by different periodic orbits. For the satellite island states (figure 8(*e*)) the rescaled eigenphases fall almost exactly along straight lines on the integers. This can be explained by the fact that the periodic orbit is stable and that the nearby phase space is near-integrable. In contrast, the period-4 and period-5 orbits are unstable, and so their respective scarred eigenvectors interact with other states via avoided crossings. This is most apparent for the period-4 orbit, for which one observes in figure 8(*c*) rather orderly fluctuations around the horizontal, suggesting some kind of beat phenomena with a nearby periodic orbit with almost the same value of λ/T.

Another difference is the following: From figure 8 it is apparent that the period-4 and period-5 unstable periodic orbits support $\sim 2T$ scarred eigenvectors, while the period-6 stable orbit clearly supports only T eigenvectors. This can be explained by the fact that the period-6 orbit is self-retracing, while the period-4 and period-5 orbits are not. If an orbit is not self-retracing, it has a distinct time-reversed partner, which of course has the same action and stability. Throughout we have observed that the behaviour of 'regular' eigenvectors and scarred eigenvectors differ in degree rather than quality, and so it should not perhaps come as a surprise to learn that scarred eigenvectors can appear in pairs, in much the same way as the regular eigenvectors appear in tunnelling pairs [40].

We demonstrate this fact more explicitly in figure 9, where we display the (rescaled) eigenphases of the 11 eigenvectors which are most scarred by the period-5 periodic orbit, at $k = 600$. Additionally, we differentiate between symmetric and antisymmetric eigenvectors by denoting the former by open squares and the latter by full circles. One can see that, out of the 11 most-scarred eigenvectors, 10 arrange themselves along the now familiar integer ξ values. Moreover, one can clearly see that the eigenvectors come in symmetric/antisymmetric doublets. The separation between the pairs is displayed in the inset, along with a line denoting the mean level spacing of the chaotic layer estimated from the eigenvector entropies (see figure 2). Interestingly, the typical 'splitting' of the scarring doublets is larger than the mean level spacing. This is to be expected, since both the orbit and its time-reversed image reside in the same chaotic layer, and are not separated by any well formed classical transport barriers. Nevertheless, the scarring doublet is clearly well defined.

Scarring eigenvector doublets are expected to give rise to scarred eigenfunction doublets in the same manner as tunnelling eigenvector doublets yield tunnelling eigenenergy doublets [28]. To the best of our knowledge, this is the first time the phenomenon of scarring doublets has been described.

Finally, let us track the energy evolution of the eigenvectors which are scarred by the unstable period-5 orbit, for which the eigenphases were displayed above. The periodic orbit itself is shown in figure 10(*a*). It is not a self-retracing orbit, and so on the Poincaré cell the orbit and its time-reversed partner are distinct, and we expect to see eigenvectors which are peaked at 10 different points. In figures 10(*b*)–(*f*) we show HPDs of eigenvectors which are scarred at this pair of periodic orbits, for wavenumbers which range from $k = 110$ to $k = 600$. Scarring along this orbit first becomes unambiguously visible at $k = 110$ (figure 10(*b*)), where, however, one cannot resolve too much detail because the wavelength is too long. We next show two different scarred eigenvectors which coexist at wavenumber

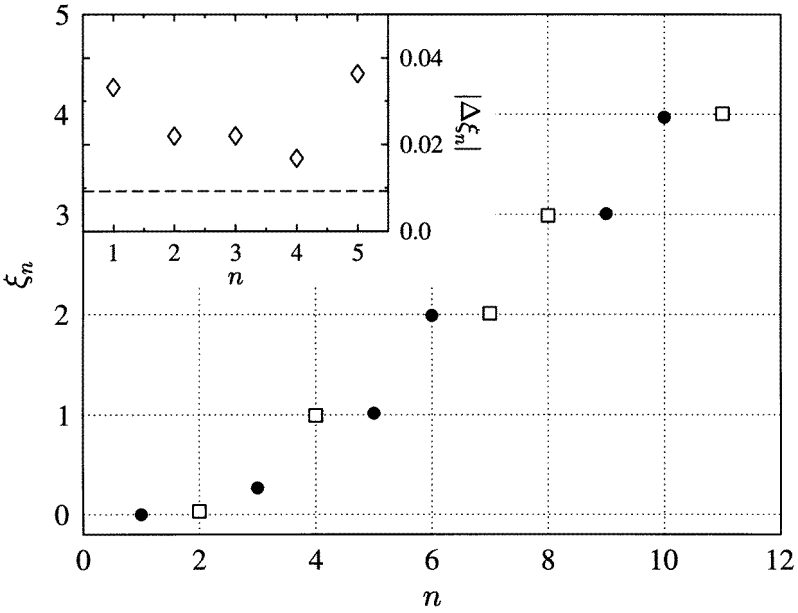

Figure 9. The rescaled eigenphase, ξ_n (see (18)), of the 11 eigenvectors which are most scarred by a period-5 non-retracing unstable periodic orbit, at $k = 600$. The orbit is the one displayed in figure 10(a). The open squares denote symmetric eigenvectors, and the full circles denote antisymmetric eigenvectors. Inset: the spacing between the rescaled eigenphases constituting the plateaus. The broken line represents the mean level spacing associated with the chaotic layer.

$k = 152.2$ (figures 10(c) and (d)). Examining figure 8(a) we see that at this wavenumber the eigenphase of one of the scarred eigenvectors (in this case the one whose HPD is displayed in figure 10(c)) is equal to an integer multiple of 2π, and so we expect a scarred quantized wavefunction there. At this wavenumber more detail is becoming visible, and the contributions of the periodic orbit and its time-reversed partner are starting to be resolved. The structure that emerges is explained in figure 10(d). This depicts another eigenvector which is also evaluated at $k = 152.2$, but whose eigenphase is $(3 \times 2\pi/5) \bmod 2\pi$, and so does not represent a quantized eigenfunction. On top of this graph we overlaid white lines which trace the stable and unstable manifolds of the periodic orbit. It is apparent that the probability peaks in the HPD align themselves with the stable and unstable manifolds. Moreover, while in figure 10(c) the probability maxima were at the periodic orbit itself, in figure 10(d) we observe a higher amplitude at the intersections of the manifolds of the periodic orbit and its time-reversed partner. Thus in cases where the periodic-orbit points are closely spaced on the Poincaré cell, and the wavelength is not too short, one can expect interference phenomena to give rise to various kinds of fine structures in the close vicinity of the orbit.

Going to higher energies, we show eigenvectors which are scarred on the same orbit at $k = 200$ (figure 10(e)) and $k = 600$ (figure 10(f)). As the wavelength decreases, interference between different probability peaks becomes less important, and the distinct maxima are more apparent. It is evident that the fundamental structure of the scarred eigenvectors persists in a distinct manner over a very wide energy range—between $k = 110$ and $k = 600$ there are more than 70 000 intervening quantized levels of the billiard.

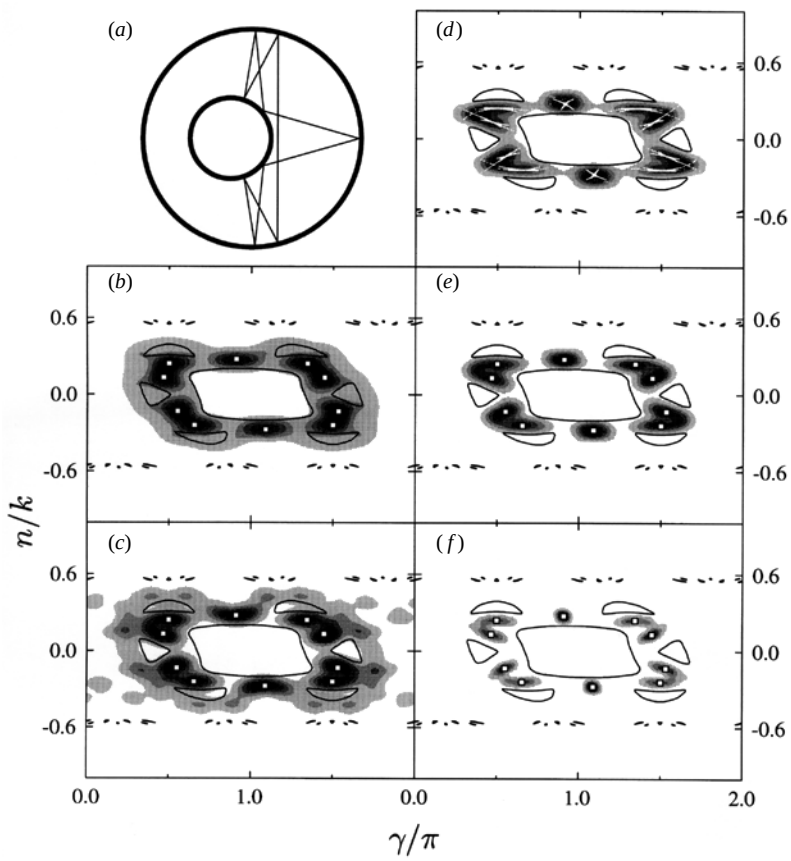

Figure 10. (*a*) The configuration-space structure of the period-5 unstable periodic orbit. (*b*)–(*f*) The HPDs of eigenvectors which are scarred by this periodic orbit, for $k = 100$ (*b*), $k = 152.2$ ((*c*) and (*d*)), $k = 200$ (*e*) and $k = 600$ (*f*). The projection of the periodic orbit and its time inverse onto the Poincaré cell is shown by open squares, and the full lines delimit the sizeable classical regular islands in the Poincaré surface-of-section. In (*d*) we also show by open areas the Poincaré cell projection of the stable and unstable manifolds of the periodic orbit.

6. Discussion

The scattering matrix **S** and its close relation the T-matrix have been used in the last few years to quantize several families of chaotic systems, most notably billiards [20, 41, 42]. In this work we have shown that the *eigenvectors* of **S** are also interesting objects of study in their own right. We described how one can project the eigenvectors onto the same Poincaré surface-of-section that is used to construct **S**, thus obtaining a phase-space picture of eigenstructures which is analogous to the familiar classical Poincaré cell pictures. We then studied the structures that emerge and their evolution in energy, and discussed their relation to the structure of quantized wavefunctions.

The main tool used in this work was the WPD and its smoothed partner the HPD, which were also utilized in [25] and are analogous to the familiar Wigner and Husimi distributions over phase space. However, the analogy does not imply an identity. The time-independent Schrödinger equation for a compact system can be solved only at quantized

values of the energy, and even then has only one single associated eigenfunction at a given quantized energy (barring degeneracies). In contrast, the S-matrix is well defined and can be decomposed into its eigenparameters at any energy. The eigenvectors of $\mathbf{S}$ therefore comprise a much richer field for research than the eigenfunctions of the Hamiltonian. Moreover, studying $\mathbf{S}$ enables one to explore the evolution of quantum phase-space structures in energy, since one can then smoothly track a structure in energy even when it does not manifest as a quantized state.

A fortuitous property of the WPD/HPDs is the ease by which they may be calculated. One simply has to evaluate $\mathbf{S}$, diagonalize, and Fourier transform, to obtain a full phase-space picture. In contrast, in order to obtain the Wigner function of a given eigenstate, Ψ, of the Hamiltonian one has to first search for the quantizing energy and then evaluate it over configuration space. This entails both a calculation of the coefficients of an expansion of Ψ over some basis, and the summation of the resulting series over a fine enough grid. This is not only time-consuming but can give rise to problems of numerical stability. For example, in the annular billiard it is natural to use polar coordinates and a basis of cylindrical incoming and outgoing waves. However, the resulting Hankel function series become increasingly ill-conditioned as the energy increases. The consequence is that, even given the coefficients of the cylindrical wave expansion to double-precision (about 15 digit) accuracy, one can directly evaluate the wavefunction over configuration space only up to $k \sim 90$. Even at lower energies the conditioning of the Hankel series is heavily dependent on, for example, the choice of the origin of the coordinate system and the method of summation. In contrast, the evaluation of HPDs entails no significant numerical problems apart from the size of the S-matrix, and we encountered no difficulty in obtaining HPDs at wavenumbers of $k = 600$ and beyond.

A new result which has emerged from this work is the appearance of *scarring doublets*. These are pairs of eigenvectors, one symmetric and one antisymmetric, which are structured by both a non-self-retracing periodic orbit and its time-reversed image, and which give rise to closely spaced pairs of structured eigenfunctions of the billiard. This effect was anticipated for states structured by a stable periodic orbit, since then the orbits are separated by classically impenetrable KAM-like tori, and the effect is a manifestation of chaos-assisted tunnelling [40]. However, its appearance for unstable scarring orbits was a surprise. It raises several interesting questions, most notably the determination of the statistics of the pair separation, which is not determined here by a tunnelling amplitude but by the quantum dynamics itself.

The result of this work is a new picture of the way structured states form and quantize. The philosophy is that a full set of structured eigenvectors 'exist' for all energies, and that their structure, as it manifests in the HPD, is only slowly varying with the energy. Quantization, on the other hand, is determined by the behaviour of the associated eigenphases. Regarding eigenvectors which are structured by a periodic orbit (stable or unstable) of length λ and Poincaré map period T, our results suggest that they appear in T- or $2T$-tuples, and that their associated eigenphases form a regularly spaced 'comb' of phases, with each branch increasing linearly with k with a slope of λ/T. A given structured eigenvector will consequently give rise to a structured quantized wavefunction at regular k intervals of T/λ, whenever its eigenphase passes through an integer multiple of 2π, while the family as a whole will produce either single-structured states or pairs of structured states at the EBK-like intervals of $1/\lambda$. The question of quantization is, therefore, disentangled from the one of wavefunction structure, and the two can be studied separately.

The numerical results presented here were for a billiard system, for which the classical dynamics do not depend on the energy except through a trivial scaling. In a non-scaling

system one would not expect the quantum structures to persist over 'classical' energy ranges, i.e. ranges over which the classical structures and orbits change significantly. However, at high energies there is a clear separation of scales between this classical scale and the quantum scale of the mean level separation. Therefore, we expect our conclusions to hold in non-scaling systems over energy ranges which are, in this respect, classically small but quantum-mechanically large.

An interesting note is the following. In [9] Müller and Wintgen studied the diamagnetic Kepler problem, and one of their conclusions was 'scars are the rule rather than the exception'. In contrast, in [25] Klakow and Smilansky claimed, on the basis of the Shnirelman theorem [43], that 'scars are scarce' (see also [44]). Without claiming to prove anything, our experience so far with the annular billiard tends towards the former statement, at least if scarring is determined using the HPD. For example, at $k = 600$ there are ~ 500 eigenvectors which are supported by the chaotic region of phase space, and we have come across only a few which are not manifestly peaked around some classical structure. A phenomenon which we have observed, however, is the one of mixing of two or more structured eigenvectors to yield a doublet which has a significant overlap with the supporting phase-space regions of all the constituent elements. Additionally, an eigenvector may be structured not only by a periodic orbit but also along its stable/unstable manifolds, and in particular at the major homoclinic intersections. The result is that it is not always straightforward to tell if a given state is structured or not. Some evidence of this fact can even be seen in [10, figures 1(a) and (b)]. There, the authors claim to have found only a low density of scarred states; however, they comment about the filamentary and non-ergodic nature of the smoothed Wigner functions of the states which they identify as 'almost microcanonical', i.e. not clearly structured.

The work we report on here is preliminary, and much of the evidence is numerical in nature. However, one can think of various implications concerning the creation of quantum phase-space structures. Most importantly, it seems that the eigenfunction structuring over an energy range which is much larger than the mean level spacing can be determined by examining the eigenvectors of $\mathbf{S}$ at any *single* intermediate energy, which does not even have to be an eigenenergy of the system. This would imply that the interference effects between different periodic-orbit (more precisely, composite-orbit) contributions considered in [25], cannot be very important, since one would expect them to be strongly energy dependent. Indeed, in our opinion structuring of wavefunctions is best studied in the *time* (or time-like) domain; the structuring of S-matrix eigenvectors is not significantly energy dependent over quantum energy scales, and the behaviour of the associated eigenphases is even simpler, a linear increase with k with a classically determined slope. Thus periodic-orbit theory, in spite of its successes [18, 19, 25], is perhaps not the optimal way to proceed.

One can think of many open questions posed by the current work. Ideally, one would like to understand the structuring of eigenvectors from a semiclassical point of view. The curious phenomenon of the T-multiplicity of eigenvectors which are scarred by a period-T orbit also remains to be understood, as does the existence of 'excited scars'. Scarring doublets also seem to raise more questions than they answer, such as the values of the pair separations and the manner in which the doublet evolves under the application of a magnetic field. Another interesting quantity is the 'scarring observable' $\mathcal{B}(\alpha)$. It would be interesting to develop a semiclassical theory for $\mathcal{B}(\alpha)$, and compare it with the scarring criterion developed in [18] to see similarities and differences. Finally, one can study the interactions and mixing between different structured states, especially in the limit of high energy.

Acknowledgments

It is our pleasure to thank Professor H A Weidenmüller for his support and encouragement, as well as useful discussions. This work was partially funded by a Minerva fellowship.

References

[1] McDonald S W 1983 *PhD Thesis* Lawrence Berkeley Laboratory *Preprint* LBL 14837
[2] Heller E J 1984 *Phys. Rev. Lett.* **53** 1515
[3] Sridar S 1991 *Phys. Rev. Lett.* **67** 785
[4] Fromhold T M *et al* 1995 *Phys. Rev. Lett.* **75** 1142
[5] Wilkinson P B *et al* 1996 *Nature* **380** 608
[6] Waterland R L *et al* 1988 *Phys. Rev. Lett.* **61** 2733
[7] Eckhardt B, Hose G and Pollak E 1989 *Phys. Rev.* A **39** 3776
[8] Wintgen D and Hönig A 1989 *Phys. Rev. Lett.* **63** 1467
[9] Müller K and Wintgen D 1994 *J. Phys. B: At. Mol. Opt. Phys.* **27** 2693
[10] Prosen T and Robnik M 1993 *J. Phys. A: Math. Gen.* **26** 5365
[11] Provost D and Baranger M 1993 *Phys. Rev. Lett.* **71** 662
[12] de Polavieja G G, Borondo F and Benito R M 1994 *Phys. Rev. Lett.* **73** 1613
[13] Li B and Robnik M 1995 *J. Phys. A: Math. Gen.* **28** 2799
[14] Bogomolny E B 1988 *Physica* **31D** 169
[15] Berry M V 1989 *Proc. R. Soc.* A **423** 219
[16] Feingold M *et al* 1990 *J. Phys. A: Math. Gen.* **146** 199
[17] Feingold M 1994 *Z. Phys.* B **95** 121
[18] Agam O and Fishman S 1994 *Phys. Rev. Lett.* **73** 806
[19] Fishman S, Georgeot B and Prange R E 1996 *J. Phys. A: Math. Gen.* **29** 919
[20] Doron E and Smilansky U 1992 *Nonlinearity* **5** 1055
[21] Bogomolny E B 1992 *Nonlinearity* **5** 805
[22] Marcus R A 1971 *J. Chem. Phys.* **54** 3965
[23] Miller W H 1974 *Adv. Chem. Phys.* **9** 48
[24] Blümel R and Smilansky U 1990 *Phys. Rev. Lett.* **64** 241
[25] Klakow D and Smilansky U 1996 *J. Phys. A: Math. Gen.* **29** 3213
[26] Dietz B and Smilansky U 1993 *Chaos* **3** 581
[27] Bohigas O, Boosé D, Egydio de Carvallho R and Marvulle V 1993 *Nucl. Phys.* A **560** 197
[28] Doron E and Fischat S D 1995 *Phys. Rev. Lett.* **75** 3661
[29] Li B and Robnik M 1995 *J. Phys. A: Math. Gen.* **28** 4843
[30] Smilansky U 1991 *Proc. 1989 Les Houches Summer School on 'Chaos and Quantum Physics'*, ed M-J Giannoni, A Voros and J Zinn-Justin (Amsterdam: Elsevier) p 371
[31] Frischat S D and Doron E. Unpublished
[32] Peres A 1991 *Adriatico 1990 Research Conference and Miniworkshop on 'Quantum Chaos'* ed H A Cerdeira, R Ramaswami, M C Gutzwiller and G Casati (Singapore: World Scientific) pp 73–110
[33] Averbukh V, Moiseyev N, Mirbach B and Korsch H 1995 *Z. Phys.* D **35** 247
[34] Porter C E 1965 *Statistical Theory of Spectral Fluctuations* (New York: Academic)
[35] Bohigas O, Tomsovic S and Ullmo D 1990 *Phys. Rev. Lett.* **65** 5
[36] Utermann R, Dittrich T and Hänggi P 1994 *Phys. Rev.* E **49** 273
[37] Baltes H P and Hilf E R 1976 *Spectra of Finite Systems* (Mannheim: Bibliographisches Institut)
[38] Smilansky U 1995 *Proc. 1994 Les Houches Summer School on 'Mesoscopic Quantum Physics'* ed E Akkermans, G Montambaux, J-L Pichard and J Zinn-Justin (Amsterdam: Elsevier) p 373
[39] Sommerfeld A 1964 *Lectures on Theoretical Physics* vol 6 (New York: Academic)
[40] Bohigas O, Tomsovic S and Ullmo D 1990 *Phys. Rev. Lett.* **64** 1479
[41] Bogomolny E B 1990 *Comm. At. Mol. Phys.* **25** 67
[42] Rouvinez R and Smilansky U 1995 *J. Phys. A: Math. Gen.* **28** 77
[43] Shnirelman A I 1974 *Usp. Mat. Nauk.* **29** 181
[44] Li B and Robnik M 1994 *J. Phys. A: Math. Gen.* **27** 5509